Numerical simulation of Japan Sea effect snowfall

By M. A. ESTOQUE, *Rosenstiel School of Marine and Atmospheric Science, University of Miami, Coral Gables, Florida, USA* and
K. NINOMIYA, *Meteorological Research Institute, Tokyo, Japan*

(Manuscript received May 20; in final form September 22, 1975)

ABSTRACT

Snowfall associated with the modification of cold air-mass outbreaks by the Sea of Japan is simulated with a simple numerical model. The model incorporates the effects of momentum, heat, and moisture fluxes across the air–sea interface as well as the effects of orography. The simulated distributions of snowfall, temperature, wind, and moisture are compared with observations and reasonable agreement is found. Numerical experiments were made in order to determine the dependence of the snowfall distribution on the large scale prevailing conditions. The results indicate that the occurrence of snowfall is controlled primarily by orographic lifting. An unexpected finding is that the snowfall distribution is not very sensitive to the dryness of the prevailing flow.

1. Introduction

During the winter monsoon season in the Far East, snow frequently falls over the mountains of Central Japan and the adjacent coastal areas of the Japan Sea. An indication of the geographical distribution of the snowfall during the season is shown in Fig. 1.1; for comparison, the corresponding distribution over the Sea of Japan is presented in Fig. 1.2. It may be noted that the largest amounts of precipitation occur over the Japan Sea coastal regions and the mountain regions while smaller amounts occur over the sea to the northwest and the leeside plains to the southeast. Since the monsoon flow has a predominantly northwesterly component and since the Central Japan mountains are roughly normal to this flow, the precipitation distribution appears to be due primarily to orographic lifting. The cold airmass from the Asian continent picks up heat and moisture as it flows over the warm sea of Japan (e.g. Asai, 1965; Ninomiya, 1968). This addition of heat and moisture makes the airmass relatively unstable and cumulus clouds develop remarkably over the coastal area where the warm Tsushima current flows. The condensation and precipitation are especially enhanced where the airmass is lifted by the mountains. This process appears to be the dominant mechanism for explaining the precipitation distribution in Fig. 1.1. According to Fukuda (1965) and Matsumoto et al. (1965, 1967), heavy snowfall occurs over the Japan Sea coastal areas due to the smaller-scale low-level disturbances. The disturbances usually develop within the northwest monsoon airmass over these areas when the temperatures in the overlying middle troposphere are unusually low. Although the amount of precipitation due to these disturbances is by no means negligible, it is considerably smaller, in the mountain regions, than that due to orographic lifting.

The snowfall described above, which is associated with the Siberian northwest monsoon, is somewhat similar to the so called lake-effect snowfalls over the Great Lakes of the United States; these occur during cold air-mass outbreaks. Over both Japanese and United States areas, the snowfall occurs after cold airmasses are heated and moistened as they flow over the warm water surfaces. However, the precipitation mechanisms are somewhat different. In Japan, especially over the mountain regions, the primary mechanism is orographic lifting. Over the United States Great Lakes region where high mountains do not exist, however, the primary mechanism is upward motion due

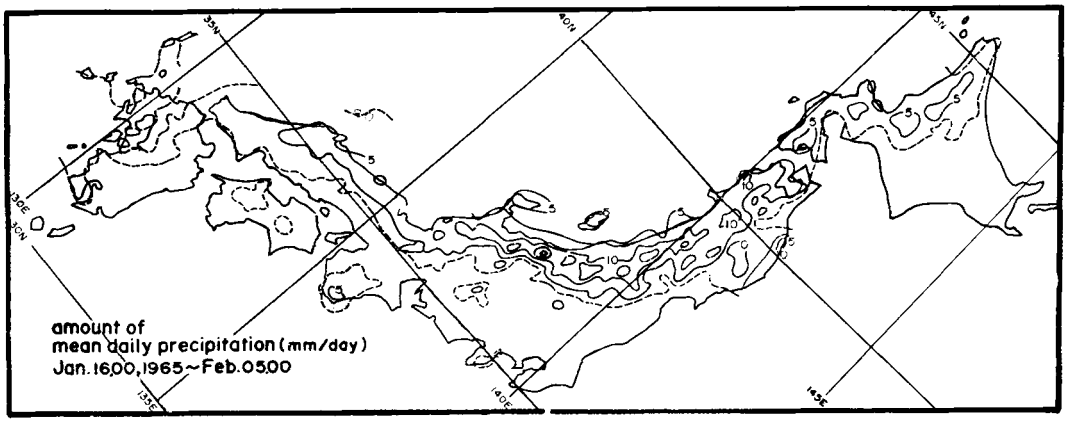

Fig. 1.1. The distribution of the mean daily precipitation over the Japan Islands for January 16–26, 1963, January 16–February 5, 1964 and January 16–February 5, 1965.

to lake-induced mesoscale disturbances. These disturbances are generally intense when the low-level prevailing flow has a long trajectory over water and when the temperature in the middle troposphere is low. The nature of these disturbances could be similar to the small-scale disturbances along the Japan Sea coastal areas described by Fukuda and Matsumoto et al. (op. cit.). The lake-effect snowfalls have been simulated rather successfully with a simple numerical model by Lavoie (1972). The model has also been applied to study the trade wind weather on Oahu Island (1974). It would be interesting to find out whether the same model could also simulate the Japan Sea effect snowfall. In this paper, we present the results of such an attempt.

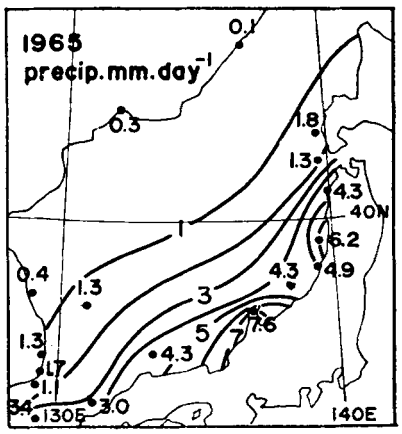

Fig. 1.2. The distribution of the mean daily precipitation for the winter of 1965.

2. The model and the numerical experiments

The model has been described in detail previously by Lavoie (1972); it is, therefore, sufficient in this paper to present only the important aspects of the model. The model is the equivalent of a one-layer (well-mixed layer) primitive equation model. The primary dependent variables of the model are those which describe the properties of the layer. These are: horizontal wind vector ($\mathbf{V}$), potential temperature (θ), mixing ratio (q), depth of the well-mixed layer (h), vertical velocity (w) and the precipitation rate (M). The first four variables are obtained with the aid of the following prediction equations:

$$\frac{\partial \mathbf{V}}{\partial t} = -\mathbf{V}\cdot\nabla\mathbf{V} - f\mathbf{K}x\mathbf{V} - \mathbf{F}_t - (h_t - h) f\mathbf{K}x \times \frac{\partial \mathbf{V}_g}{\partial z} + \frac{g}{\theta_h}\left[\theta - \theta_h - \Gamma - \frac{(h_m - h_t)}{4}\right]\nabla h + \frac{g}{2\theta}(h - z_s)\nabla\theta - \frac{C_D}{h - z_s}|\mathbf{V}|\mathbf{V} \quad (1)$$

$$\frac{\partial \theta}{\partial t} = -\mathbf{V}\cdot\nabla\theta + \frac{C_D}{h - z_s}|\mathbf{V}|(\theta_0 - \theta) + \frac{L\theta\bar{\alpha}M}{C_D\bar{T}(h - z_s)} \quad (2)$$

$$\frac{\partial q}{\partial t} = -\mathbf{V}\cdot\nabla q + \frac{C_D}{h-z_s}|\mathbf{V}|(q_0-q) - \frac{\beta|w_h|(q-q_h)}{h-z_s} - \frac{\bar{\alpha}M}{h-z_s} \quad (3)$$

$$\frac{\partial h}{\partial t} = -\mathbf{V}\cdot\nabla h + w_h + \left(\frac{1}{\Gamma}\frac{\partial\theta}{\partial t}\right)_{\theta=\theta_h} \quad (4)$$

where $\mathbf{F}_i \equiv \theta/\theta_h(\alpha\nabla p)_h$ at the initial time. In the above equations, the quantities are denoted by the customary meteorological notation. The geostrophic wind shear, $\partial\mathbf{V}_g/\partial z$, is that which corresponds to the region above the well-mixed layer; Γ is the potential temperature lapse rate in the same upper layer. The subscript, h, refers to values at the top of the well-mixed layer and the subscript, i refers to the value at $t=0$. The subscript, 0, indicates values at the ground while, s indicates value at 50 m above the ground (top of the constant flux layer). The overbar means vertical average. The constant, β, is a model parameter which specifies the intensity of mixing at $z=h$. Finally, the subscript, $\theta=\theta_h$, means that the term is computed only if $\theta=\theta_h$.

The remaining variables, w and M, are calculated with the aid of the following diagnostic equations.

$$w_h = \{\mathbf{V}\cdot\nabla z_0[1+g(h-z_s)/2c^2] - (h-z_s)\nabla\cdot\mathbf{V}\}/[1-g(h-z_s)2c^2] \quad (5)$$

$$M = a(\varepsilon w_{cb}+1)(D-k^2) \quad (6)$$

Here, c is the speed of sound and w_{cb} is the vertical velocity at cloud base. The other undefined quantities (a, ε, D, and k) are model parameters. Eq. (5) is derived from a simplified form of the equation of continuity while eq. (6) is an empirical relationship.

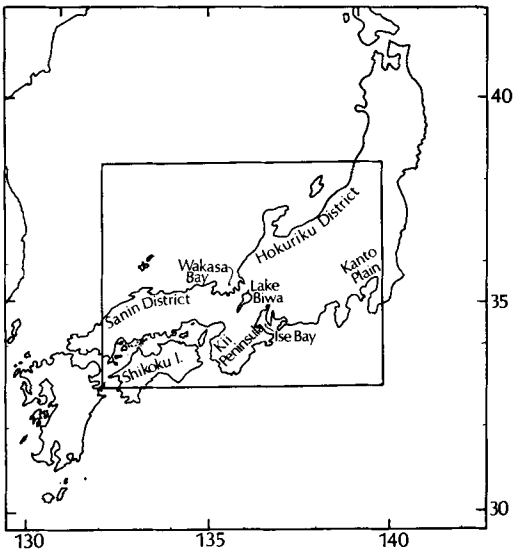

Fig. 2.1. The domain of integration is indicated by the large rectangle. The inner rectangle indicates the fine mesh region ($\Delta x = \Delta y = 20$ km).

The model equations were integrated numerically for the region enclosed by the larger rectangle in Fig. 2.1. A rectangular grid was used with equally-spaced (20 km) points inside the inner rectangle; outside it, the grid distance increases geometrically towards the outer rectangle. Details concerning the formulation of the initial and the boundary conditions, as well as the method of numerical integration, are described in the reference cited and will not be repeated here.

In order to analyze the performance of the model, we made seven numerical experiments. For purposes of discussion, the first experiment

Table 1. *Characteristics of the Numerical Experiments*

Expt. no.	Initial wind speed, m sec^{-1}	Initial wind direction	Initial mixing ratio, g/kg	Land R.H., %	C_D at sea
1 (Control)	10	NW	1	35	1.5×10^{-3}
2	10	WNW	1	35	1.5×10^{-3}
3	10	NNW	1	35	1.5×10^{-3}
4	15	NW	1	35	1.5×10^{-3}
5	10	NW	0.5	35	1.5×10^{-3}
6	10	NW	1	50	1.5×10^{-3}
7	10	NW	1	35	3.0×10^{-3}

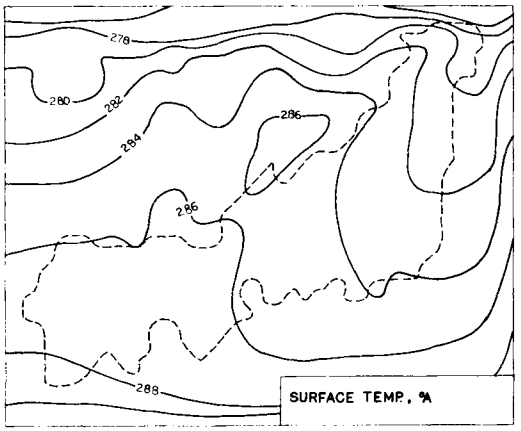

Fig. 2.2. The lower boundary distribution for temperature.

is designated as the control experiment because it represents an attempt to simulate an actually-observed meteorological situation. Each one of the other six experiments differs from the control experiment in only one aspect concerning either the initial condition, boundary condition, or the value of the drag coefficient over the sea. By varying the initial condition, one is able to simulate different large scale prevailing conditions (upstream). The characteristics of the different experiments are summarized in Table 1.

Experiments 1, 2, and 3 were designed for the purpose of assessing the effect of varying the direction of the prevailing flow. Experiment 4 differs from the control experiment in the wind speed. Therefore, by comparing the results of the integrations for both experiments, one can determine the effect of the wind speed. In a similar manner, one can assess the effect of a drier atmosphere with the aid of Experiment 5. One of the somewhat arbitrary conditions used in the integration is the specification of the relative humidity at the earth's surface. The specified relative humidity, together with the surface temperature, enables one to compute the boundary value for mixing ratio, q_0, at the ground surface. There is some uncertainty in the prescription of the relative humidity. In order to determine the sensitivity of the integration results to the assumed value of the relative humidity, we used a larger value in Experiment 6. Finally, since there is also an uncertainty in the value of the drag coefficient, we made Experiment 7 for the purpose of determining the sensitivity of the results to a larger value of C_D at sea.

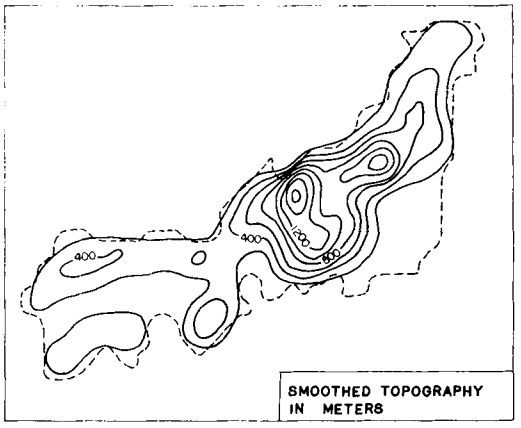

Fig. 2.3. The distribution of surface elevation.

The integrations require the specification of the lower boundary values, θ_0, and q_0. The boundary values for θ are obtained from Fig. 2.2. The sea surface isotherms in this figure are based on climatological values; for simplicity, the land surface isotherms were drawn by simply connecting with smooth lines the appropriate sea surface isotherms ending at opposite shorelines. The surface values for mixing ratio are obtained by assuming a sea surface relative humidity of 100% and a ground surface relative humidity of 35% (50% for Experiment 6). In addition to these surface conditions, we specified the height of the terrain shown in Fig. 2.3. The heights were obtained by smoothing the heights at individual grid points which were obtained from topographic maps. The smoother is the 9-point weighting operator used by Lavoie (*op. cit.*); the operator was used successively for two times. For simplicity in the integrations, Kyushu Island is replaced by a flat ocean surface.

The geostrophic wind shear above the mixed layer was prescribed to be as follows:

$$\frac{\partial u}{\partial z} = 6 \text{ m sec}^{-1} \text{ km}^{-1} \qquad \frac{\partial v}{\partial z} = 2 \text{ m sec}^{-1} \text{ km}^{-1}$$

The other model parameters are the same as those used by Lavoie (*op. cit.*).

The initial conditions were assumed to be uniform throughout the region of integration. The specific values for $\mathbf{V}$ and q are already given in Table 1. For θ and h, the values are 263° A and 2 km, respectively.

3. Results of numerical experiment

In the present section we will discuss the results of the numerical experiments described in the previous section. The sets of the governing equations are integrated for 24 hours. The quasi-steady states are found after 8 hours and some small-scale noises begin to develop after 16 hours of integration. We will, therefore, present and discuss the calculated fields at 12 hours after initial time.

(1) *Results of "control experiment"*

The distribution of the precipitation is presented in Fig. 3.1. The amount of precipitation over the Japan Sea is about 0.01–0.02 cm/hour. The high precipitation occur over the very narrow area along the Japan Sea coast where the maximum amount is about 0.18 cm/hour, while precipitation does not occur over the lee-side of the mountains and the Pacific coastal regions. There is some precipitation (0.02 cm/hour) over the windward side of the mountains in Kii Peninsula and Shikoku Island.

The horizontal distribution of the height of the inversion base is presented in Fig. 3.2. The height of the base increases very gradually over the Japan Sea from 2 000 m over the Continent to 2 400 m over the Japan Sea coastal area. As seen in the map, the inversion base is relatively low off Sanin District. The map of the vertical velocity (not shown in the present paper) suggests that the low inversion base mentioned above may be due to the weak descending motion. The inversion base rises rapidly over the Japan Sea coastal area to the height of 2 800 m. It attains the maximum height of 3 200 m over the southwest side of the mountains. The height of the base again decreases to 2 400 m over the Pacific. This distribution of inversion height obtained from the "control experiment" indicates strong topographic influence on the inversion height.

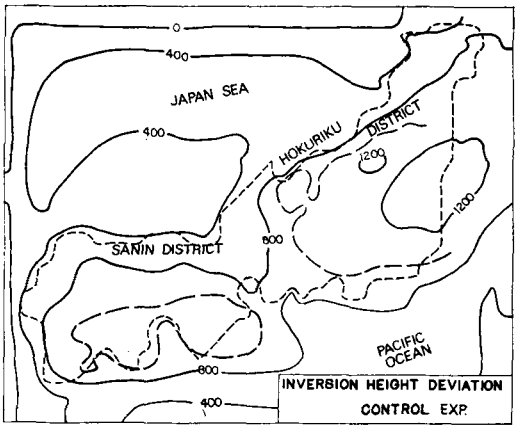

Fig. 3.2. The distribution of the height deviation of the inversion base obtained from the control experiment. Units, m.

Fig. 3.3 presents the distribution of the mean wind velocity and the relative vorticity in the mixing layer. The topographic influences of the Japan Islands on both the wind speed and direction are clearly seen in this figure. For example, the wind speed is remarkably strong along "the

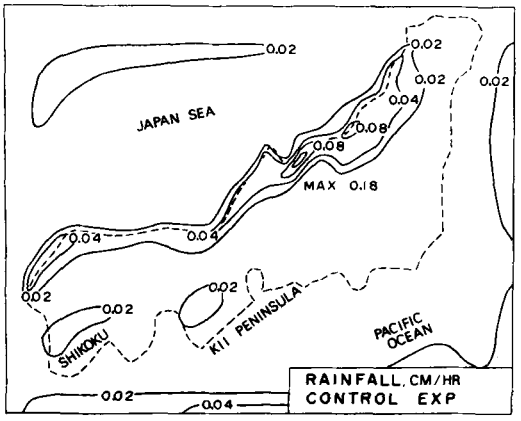

Fig. 3.1. The distribution of the precipitation obtained from the control experiment.

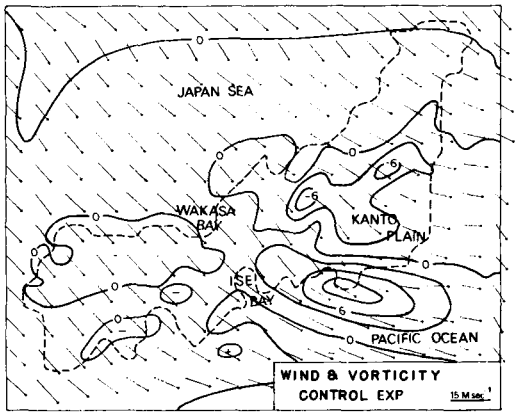

Fig. 3.3. The distribution of the mean wind velocity and the vorticity in the mixed layer obtained from the control experiment. Vorticity units, 10^{-5} sec^{-1}.

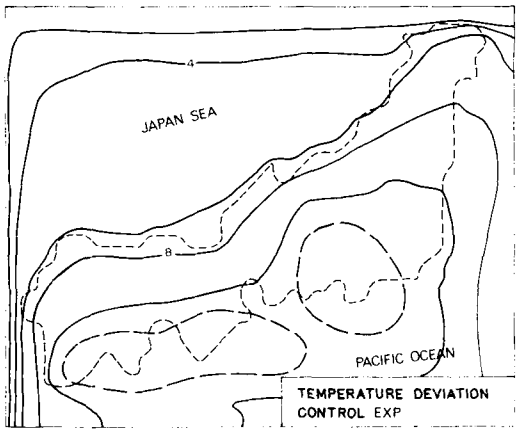

Fig. 3.4. The distribution of the mean potential temperature deviation in the mixed layer obtained from the control experiment. Units, °K.

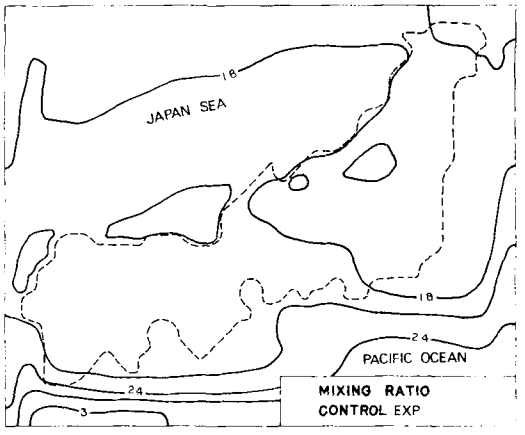

Fig. 3.5. The distribution of the mean mixing ratio of water vapor in the mixed layer obtained from the control experiment. Units, g/kg.

great valley" (which extends from Wakasa Bay to Ise Bay through Lake Biwa) while winds are very weak over Kanto Plain which is located in the lee side of high mountain ranges. These ranges tend to generate anticyclonic vorticity over them and cyclonic vorticity downwind.

Let us next examine the field of potential temperature (Fig. 3.4) and that of mixing ratio of water vapor (Fig. 3.5). The increase of the potential temperature during the air-mass passage over the Japan Sea is 6–8 K. Almost uniform distribution of potential temperature is found over the lee side of the mountains, the Pacific coastal area and over the Pacific. The increase of the mixing ratio over the Japan Sea is 0.8–1.0 g/kg. The mixing ratio is relatively small ($\sim$1.6 g/kg) over the northeastern part of the Japan Islands and relatively large ($\sim$2.0 g/kg) over the southwestern part. It increases rapidly over the Pacific and attains the value of about 3.0 g/kg off Shikoku Island.

(2) *Results of "WNW and NNW wind experiment"*

This experiment would indicate the influence of the direction change of the prevailing wind on the distribution of the precipitation over the Japan Islands. The physical parameters used in this experiment are the same as used in the control experiment except the wind direction at the initial and along the upstream boundary.

The features of the distribution of the height of the inversion base, wind velocity, potential temperature and mixing ratio resulting from these experiments are quite similar to the features of the corresponding fields obtained from the control experiment. Some differences between these experiments are, however, found on the precipitation maps. The distribution resulting from WNW wind experiment (Fig. 3.6) indicates the increase of the snowfalls along the west side of the mountains and that from NNW wind experiment (figure is not presented) indicates the increase along the north side of the mountains. From the nature of the numerical model of this study, it is natural that the area of maximum snowfalls appears over the mountains facing to the prevailing winds.

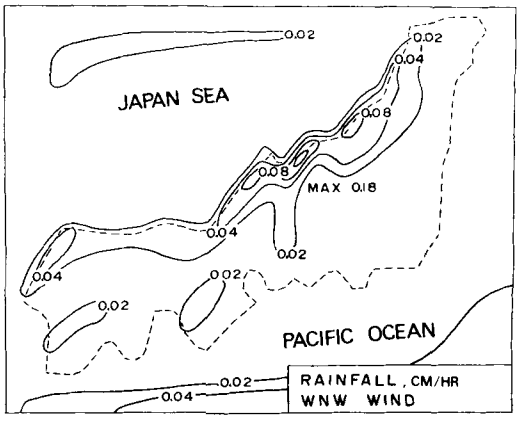

Fig. 3.6. The distribution of the precipitation obtained from the WNW wind experiment.

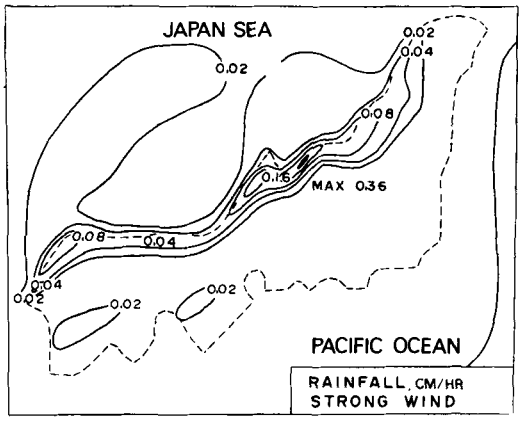

Fig. 3.7. The distribution of the precipitation obtained from the strong wind experiment.

(3) *Results of "strong wind experiment"*

The object of this experiment is to know the influence of the wind speed increase on the air-mass transformation and the snowfalls. The initial and upstream boundary value of U and V of this experiment are 10 m/sec (cf., 7 m/sec in the control experiment) and other parameters are exactly the same as these used in the control experiment. From the nature of the equation system of the model, we expect two effects of the wind speed increase. One effect is the increases of evaporation and sensible heat supply because these amounts are proportional to the wind speed. The second effect would be the increase of topographic upward motion because it is also proportional to the wind speed.

As seen in Fig. 3.7, the amount of the precipitation obtained from strong wind experiment is about twice as large as these from the control experiment although the pattern of precipitation of these experiments indicates similar characteristics.

The distribution of the height of the inversion base of this experiment is almost similar to that of control experiment although it rises more rapidly over the coastal area of Hokuriku District for the former experiment.

In spite of the increase in sensible heat supply and evaporation, the distribution of potential temperature and the mixing ratio of the strong wind experiment is not notably different from these of control experiment. This would be due to the fact that the magnitudes of thermal and moisture advection are also proportional to the wind speed and therefore the increase of the heat and moisture supply would be balanced by the advection.

(4) *Results of "small initial mixing ratio experiment"*

The "small initial mixing ratio experiment" would represent the case of cold air outbreak of a very dry airmass. The initial and upstream boundary value of mixing ratio of this experiment is 0.5 g/kg (cf. 1.0 g/kg for the control experiment).

We cannot find any significant differences between the computed fields (not shown) from this model and those from the control experiment. The amount of the precipitation is slightly small as compared with that of control experiment.

If the air-mass is very dry, we expect much evaporation from the Japan Sea because the amount of evaporation is proportional to the air–sea moisture difference. It could be said, therefore, that the initial and upstream boundary value of the mixing ratio is not the important controlling factor for the air-mass modification and the snowfall over the Japan Sea and the Japan Islands.

(5) *Results of "wetter ground experiment"*

In the "wetter ground experiment", the relative humidity at the ground surface is chosen to be 50% (cf. 35% in the control experiment). Due to the change of this parameter, some increases in the precipitation amount over the

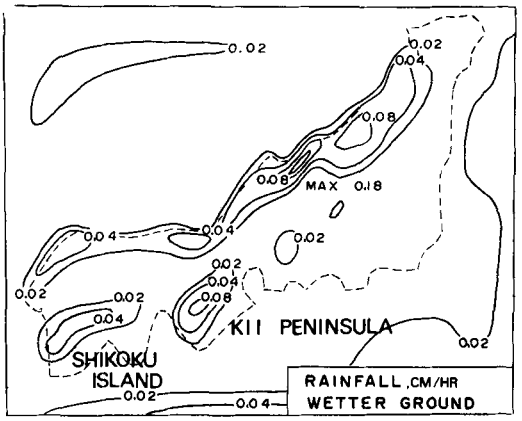

Fig. 3.8. The distribution of the precipitation obtained from the wetter ground experiment.

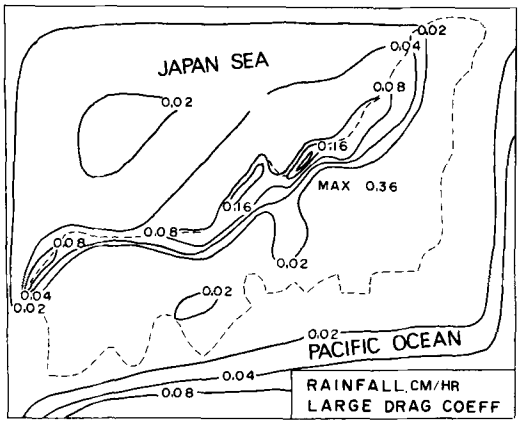

Fig. 3.9. The distribution of the precipitation obtained from the large drag coefficient experiment.

mountains in Kii Peninsula and Shikoku Island (Fig. 3.8), while the precipitation over the Japan Sea coastal area does not change.

(6) *Results of "large drag coefficient experiment"*

In the large drag coefficient experiment we use large values of the drag coefficient over the sea, which is twice as large as these adopted in the control experiment. The increase in the drag coefficient would produce large frictional force, evaporation and sensible heat supply.

The obtained field of various quantities from this experiment are considerably different from those obtained from the control experiment. The amount of precipitation (Fig. 3.9) is about twice as large as that of the control experiment. This increase would be due to the increase in the evaporation.

The increases in potential temperature and mixing ratio during the air-mass passage over the Japan Sea are about 12 K and 2.4 g/kg respectively, which are fairly larger than these resulting from the control experiment. It is found that both potential temperature and mixing ratio increase rapidly over the Pacific to the south of Shikoku Island and Kii Peninsula.

The distribution of the height of the inversion base in this experiment (Fig. 3.10) is also remarkably different from the previous experiments. The inversion base rises rapidly to 2 800 m soon after the airmass leaves the Continent. The height of inversion base is 2 800–3 200 m over the Japan Sea. The maximum height of about 3 700 m is found over Hokuriku District. The inversion base becomes gradually lower toward the Pacific side of the Japan Islands and indicates the minimum height (2 800 m) over the Pacific coastal area. Due to the large heat energy supply, the inversion base again rises over the Pacific and attains its maximum height (4 400 m) off the Japan Islands.

4. Comparison of results of experiment with observation

In the present section we will compare the results of the experiments described in the previous section with observations.

(1) *Climatological and synoptic distribution of the snowfall*

In order to compare the results of the numerical experiment with the actual features of air-mass transformation and the snowfall, we select the period between 16 January and 5 February 1965 as the period of a typical winter monsoon and the case of snowfall in 20 January 1964 as a typical example of the moderately strong cold air outbreak.

Fig. 1.2 shows the distribution of the mean amount of precipitation over the Japan Sea during the period. The amount could be estimated from this figure to be about 2 mm/day (0.01 cm/hour). The climatological and synoptic distribution of the precipitation over the

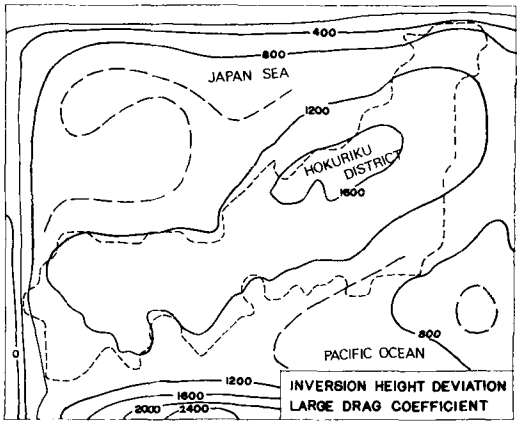

Fig. 3.10. The distribution of the height of the inversion base obtained from the large drag coefficient experiment. Units, m.

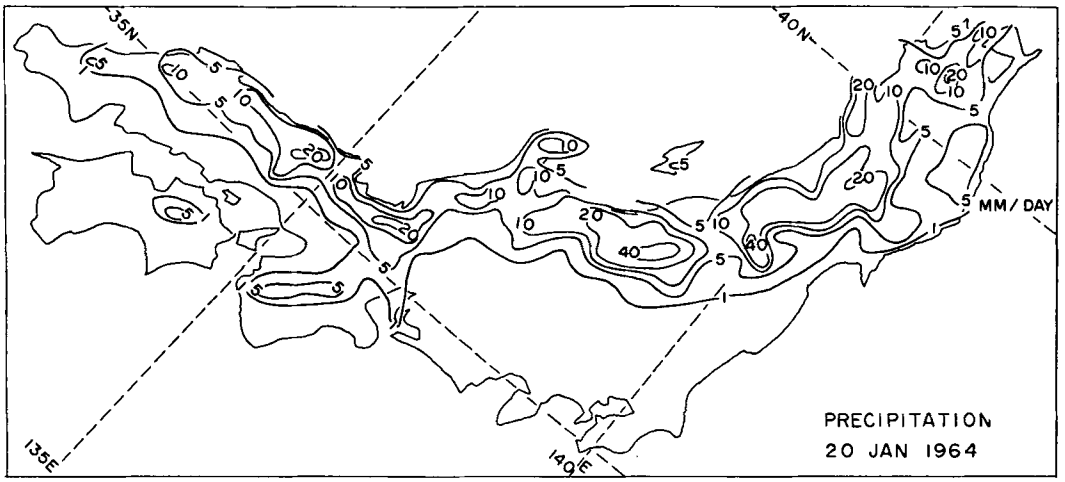

Fig. 4.1. Synoptic distribution of precipitation amount over the Japan Islands on 20 January 1964. Units, mm/day.

Japan Islands are presented in Fig. 1.1 and Fig. 4.1 respectively. By and large, the patterns of precipitation obtained from the experiments coincide well with that of observation.

As for the amount of precipitation, the results of control, NNW and WNW wind experiment coincide well with the observation. The amount of precipitation over the mountain areas in Shikoku Island and Kii Peninsula of the wetter ground experiment is much larger than observed one. This would be due to the overestimation of the evaporation from the ground surface. The amount of precipitation of both the strong wind and the large drag coefficient is about twice as large as the observed amount.

The largest disagreement between the results of experiment and observation is the location of the area of maximum snowfall. The results of experiments indicate that the strongest snowfall occurred along the coastal line, while the observed maximum snowfall areas are located over the inland areas 50–70 km far from the coastal line. This disagreement could be explained by the drift of the snowflake. Since the falling speed of snowflakes is 0.3–0.5 m/sec, it takes about 4 000 sec to fall a vertical distance of 2 000 m. This means that the snowflakes are drifted about 40 km providing that the wind speed is 10 m/sec.

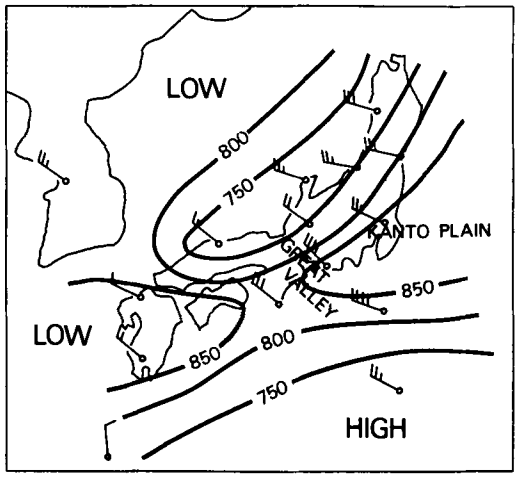

Fig. 4.2. The 900 mb wind and the height of the inversion at 1200 GST, 20 January 1964. One full barb of wind symbol equals 10 knots; inversion height, mb.

(2) *Wind velocity*

Fig. 4.2 shows the observed 900-mb winds at 1200 GST 20 January 1965. It will be found that the wind speed is relatively strong along the "great valley" and weak over the Kanto Plain. There is also an indication of a trough over the Pacific Coastal region. These features of wind speed are also well simulated by the experiment.

(3) *Distribution of the height of inversion base*

The distribution of the height of the inversion base at 2100 GST 20 January is presented

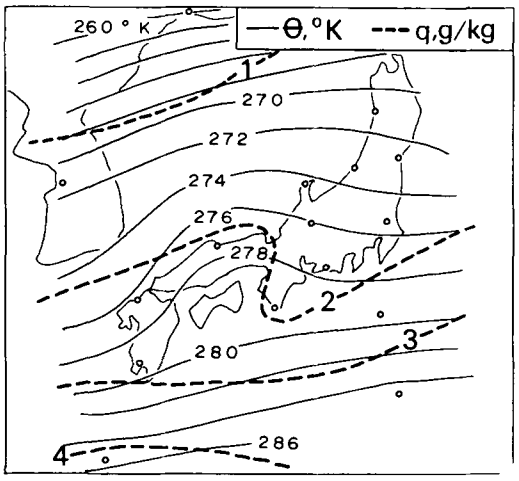

Fig. 4.3. The mean potential temperature and the mixing ratio in the layer below the inversion base at 1200 GST, 20 January 1964.

in Fig. 4.2. The inversion base indicates the maximum height of 730 mb over the Japan Sea coastal area and minimum height of 850 mb along the Pacific coastal area. The height again increases to 750 mb over the Pacific to the south of the Japan Islands.

As described in section 3, the results of all the experiments (except the large drag coefficient experiment) do not agree well with the observations; these results show the maximum height over the lee side of the mountains. The results of only the large drag coefficient experiment simulate well the characteristic features of the observations.

(4) *Distributions of the potential temperature and the mixing ratio*

The distributions of the mean potential temperature and mixing ratio in the layer below the inversion base at 1200 GST 20 January are presented in Fig. 4.3.

The observed horizontal gradient of the potential temperature and the mixing ratio are considerably stronger than those of the control and the strong wind experiment. The results of only the large drag coefficient experiment agree fairly well with the observations.

We also find important disagreements between the observed vertical gradient of θ and q and those of the model atmosphere. It is assumed that θ and q are uniform in the mixed layer in the model atmosphere of the experiment. In the actual atmosphere over Hokuriku District, θ increases at the rate of 3°K/1 000 m and q decreases at the rate of 1 g kg^{-1}/1 000 m.

(5) *Remarks*

The comparisons described above suggest that the results of the large drag coefficient experiment agree, on the whole, fairly well with the observations, although the amount of the precipitation is too much as compared with the observation.

One may be critical of the value of 3×10^{-3} for the drag coefficient which is too large. By comparing the amount of the evaporation or sensible heat supply evaluated from the atmospheric budget analysis with those evaluated from the bulk method, Ninomiya (1968) suggested that the value of the drag coefficient should be 2×10^{-3} over the Japan Sea in the winter season. It should be noted, however, that the sensible heat supply in the present model is not proportional to the temperature difference between the sea water and the lowest atmospheric layer but to the difference between the sea water and the mean temperature in the mixed layer. If this is taken into account, the value used in this numerical experiment would not be unreasonably large. The unreasonably large amount of the precipitation of the large drag coefficient experiment could be due to the overestimation of the topographic upward motion, because the upward motion in this model is not proportional to the $\mathbf{V}_0 \cdot \nabla Z$ but rather to $\mathbf{V} \cdot \nabla Z$.

It is also suggested in the discussion in (4) that the one-layer model for the mixed layer would not represent accurately the structure of actual atmosphere because there are large vertical gradients of q in the very thick neutral layer developed over the Japan Sea coastal region.

5. Concluding remarks

The results of the numerical integrations indicate that the model is able to reproduce many of the important features of the winter monsoon circulation over Japan and the surrounding sea. The accuracy of the predicted precipitation is rather remarkable if one considers the fact that the model is extremely simple. This is primarily an indication that the model is able

to predict snowfall induced by orography reasonably well. However, examination of the results indicate that it may not be able to predict snowfall associated with the minor disturbances described by Matsumoto et al. (1967) and Fukuda (1965) for no such disturbances apparently developed during the integration. The absence of the disturbances may be due simply to inappropriate initial conditions or incorrect model parameters. Or, it could be due to the lack of vertical resolution of the model. It is interesting to speculate whether this weakness of the model, and other deficiencies which are not mentioned here, can be remedied by minor changes in the model equations. If this can be done without unduly complicating the model, one may be able to forecast Japan Sea effect and lake effect snowfalls on an operational basis.

Acknowledgements

The study was done in connection with the Japan–U.S. Science Cooperative Program of the Office of International Programs, National Science Foundation, and the Japan Society for the Promotion of Science. Primary support for U.S. participation was given by National Science Foundation Grant No. GA 32202A no. 2 under the Oceanography Section. The authors are grateful to Ming Sen Lin who carried out the computer programming work. Numerical integrations were done at the Computing Facility of the National Center for Atmospheric Research whih is sponsored by the National Science Foundation.

REFERENCES

Asai, T. 1965. A numerical study of the air-mass transformation over the Japan Sea in winter. *J. Met. Soc. Japan 43*, 1–15.

Fukuda, K. 1965. Synoptic study on the mechanism of the heavy snowfall. *Geophys. Mag. 32*, 317–359.

Lavoie, R. L. 1972. A mesoscale numerical model of lake-effect storms. *J. Atmos. Sci. 29*, 1025–1040.

Lavoie, R. L. 1974. A numerical model of trade wind weather on Oahu. *Mon. Wea. Rev. 102*, 630–637.

Matsumoto, S., Asai, T., Ninomiya, K., Iida, M. & Takeuchi, M. 1965. Behavior of the extraordinary cold vortex over the Far East coastal area observed during the period from 22 January to 24 January 1963. *J. Met. Soc. Japan 43*, 100–115.

Matsumoto, S., Ninomiya, K. & Akiyama, T. 1967. Cumulus activities in relation to mesoscale convergence field. *J. Met. Soc. Japan 45*, 292–305.

Ninomiya, K. 1968. Heat and water budget over the Japan Sea and the Japan Islands in winter season. *J. Met. Soc. Japan 46*, 343–372.

ЧИСЛЕННОЕ МОДЕЛИРОВАНИЕ СНЕГОПАДОВ, ВЫЗЫВАЕМЫХ ВЛИЯНИЕМ ЯПОНСКОГО МОРЯ

С помощью простой численной модели моделируются снегопады, связанные с модификацией Японским морем прорывающихся холодных масс воздуха. В модель включения эффекты потоков количества движения, тепла и влаги через поверхность раздела воздух–море, также как и влияние орографии. Смоделированные распределения снегопада, температуры, ветра и влажности сравниваются с данными наблюдений и найдено их разумное согласие. Численные эксперименты были проделаны для определения зависимости распределения снегопадов от превалирующих крупномасштабных условий. Результаты указывают, что факт наблюдаемости снегопада контролируется в первую очередь орографическим подъемом воздуха. Неожиданно найдено, что распределение снегопадов не очень чувствительно к сухости превалирующего воздушного потока.